Materials Science & Engineering A 651 (2016) 848–853

Contents lists available at ScienceDirect

Materials Science & Engineering A

journal homepage: www.elsevier.com/locate/msea

# Ductile fracture of bulk metallic glass $Zr_{50}Cu_{40}Al_{10}$ under high strain-rate loading

L. Lu [a,b,c], C. Li [c,e], W.H. Wang [d], M.H. Zhu [b], X.L. Gong [a,*], S.N. Luo [b,c,**]

[a] CAS Key Laboratory of Mechanical Behavior and Design of Materials, Department of Modern Mechanics, University of Science and Technology of China, Hefei, Anhui 230027, PR China
[b] Key Laboratory of Advanced Technologies of Materials, Ministry of Education, Southwest Jiaotong University, Chengdu, Sichuan 610031, PR China
[c] The Peac Institute of Multiscale Sciences, Chengdu, Sichuan 610207, PR China
[e] College of Physical Science and Technology, Sichuan University, Chengdu, Sichuan 610064, PR China
[d] Institute of Physics, Chinese Academy of Science, Beijing 100190, PR China

ARTICLE INFO

*Article history:*
Received 16 September 2015
Received in revised form
12 November 2015
Accepted 13 November 2015
Available online 17 November 2015

*Keywords:*
Bulk metallic glass
Strain rate
Microstructure
Ductility
Spallation

ABSTRACT

We investigate dynamic fracture or spallation of a ternary bulk metallic glass, $Zr_{50}Cu_{40}Al_{10}$, under high strain-rate ($4–5\times10^5\ s^{-1}$) loading. Both incipient and full spall are achieved. Free-surface velocity histories and microstructure features of the recovered samples, such as necking, softening, microvoids, and rounded cups/cones, indicate exceptional ductility in deformation and fracture of this glass. Softening/necking is attributed to decreased glass transition temperature with increasing tension, and rounded cups/cones, to localized shear banding, void formation, and their interactions.



## 1. Introduction

Bulk metallic glasses (BMGs), also referred to as bulk amorphous metals, differ from general metals in their disordered atomic structures and multicomponent metal alloy systems, and exhibit excellent mechanical properties, such as large elastic strain and high yield strength [1–4], while their low ductility is still a concern. Copious studies have investigated their responses to loading at various strain rates, such as quasi-static or Hopkinson bar compression/tension, and planar impact. Ductile deformation and fracture under high strain-rate loading are relatively underexplored and of particular interest. Recently, macroscopic and nanoscale or atomic ductility were observed in quasi-static experiments [5–12]. In addition, high strain-rate spallation experiments were conducted to investigate Hugoniot elastic limit (HEL), spall strength, and fracture mechanisms of BMGs, mostly quinary or senary BMGs [13–17]. Such BMGs show certain ductility under high strain-rate loading, but higher ductility is desirable. In this work, we explore high strain-rate deformation and fracture of a ternary BMG, $Zr_{50}Cu_{40}Al_{10}$, with gas-gun plate impact loading and laser-velocimetry measurements. The shock-recovered samples are examined with scanning electron microscope (SEM). Both incipient and full spallation are observed. Free-surface velocity histories and microstructure features of the recovered samples, such as necking, softening, microvoids, and rounded cups/cones, indicate its exceptional ductility as a BMG. Deformation mechanisms are proposed to explain the observations.

## 2. Materials and experiments

A Zr-based BMG ingot, $Zr_{50}Cu_{40}Al_{10}$, is prepared by arc-melting mixtures of pure Zr, Cu and Al in an argon atmosphere, and then remelted and cast into a copper mold to obtain a cylindrical rod with a diameter of 10 mm. The rod is sectioned into multiple samples. The samples are disks with a diameter of 10 mm and a thickness of 1 mm. At ambient conditions, the density is measured by an Archimedean method to be $\rho_0=6.94\ g\ cm^{-3}$, the longitudinal sound speed determined from ultrasonic measurements is $C_L=4.74\ km\ s^{-1}$, Poisson's ratio is $\nu=0.37$ [18,19], and then the bulk sound speed is obtained as $C_0=4.04\ km\ s^{-1}$. The flyer plates with a 0.41-mm thickness are made of high-purity Cu, with $\rho_0=8.95\ g\ cm^{-3}$ and $C_0=3.94\ km\ s^{-1}$. Two parallel surfaces of a sample or flyer plate disk are polished to micron level or mirror

* Corresponding author.
** Corresponding author at: The Peac Institute of Multiscale Sciences, Chengdu, Sichuan 610207, PR China.
*E-mail addresses:* gongxl@ustc.edu.cn (X.L. Gong), sluo@pims.ac.cn, sluo@swjtu.cn (S.N. Luo).

http://dx.doi.org/10.1016/j.msea.2015.11.040
0921-5093/

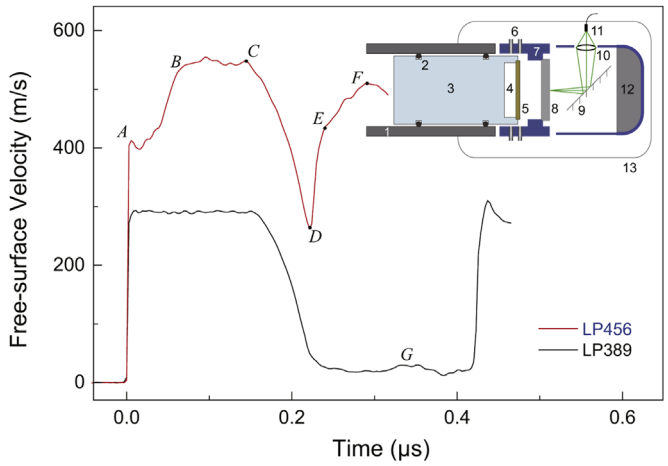


**Fig. 1.** Representative free-surface velocity–time histories of $Zr_{50}Cu_{40}Al_{10}$ BMGs under planar impact. Inset: Schematic setup for gas-gun plate-impact spallation experiments. 1: gun barrel; 2: O-ring; 3: polycarbonate sabot; 4: recess for release waves; 5: flyer plate; 6: optical fibers and detectors for the optical beam block system; 7: sample holder; 8: sample; 9: mirror; 10: lens; 11: optical fiber connected to Doppler pin system (DPS); 12: soft materials; 13: vacuum chamber.

finish.

For high strain-rate loading, flyer-plate impact experiments are conducted with a 10-mm bore, single-stage, tabletop gas gun to investigate dynamic compression and tension responses of the BMG samples. The methodology as well as data analysis related to planar impact experiments can be found in other studies [20–23]. The inset in Fig. 1 shows the schematic setup of flyer-plate planar impact experiments. A flyer plate (5) is attached to polycarbonate sabot (3), with a recess (4) immediately behind it. When a solenoid valve is fired, compressed helium is released from a high-pressure gas reservoir into the gun barrel (1), accelerating the sabot and flyer plate assembly. Upon exiting the muzzle, the flyer plate impacts the target or sample (8) under consideration. The flyer plate velocity is measured with an optical beam block system (6), and the free surface velocity of the target, with a Doppler pin system or DPS (11). A single-mode optical fiber is used as the DPS probe and collects reflected light carrying velocity information. Superposition of the Doppler-shifted light reflected from a moving interface/free surface with the reference light reflected from a static surface create interference fringes, and the beat frequency is proportional to the interface/free surface velocity. Optical signals are analyzed to deduce velocity histories via fast Fourier transformation. The muzzle, target and diagnostics are located in a vacuum chamber (13). The shocked samples are "soft" recovered with foams (12) for SEM examination.

## 3. Results and discussion

Spallation experiments are conducted at four impact velocities, 283 m $s^{-1}$, 369 m $s^{-1}$, 449 m $s^{-1}$, and 534 m $s^{-1}$, corresponding to shots LP389, LP437, LP422, and LP456, respectively. Representative free-surface particle velocity ($u_{fs}$) profiles are shown in Fig. 1. With increasing impact velocity, this BMG exhibits a transition from incipient to full spallation. For the experiment conducted at the lowest impact velocity (LP389), a single elastic shock forms. At higher impact velocities, the free-surface velocity profiles show clearly an elastic–plastic (two-wave) structure, i.e., segments *OA* (elastic) and *AB* (plastic). Segment *BC* denotes the plastic shock plateau. The Hugoniot elastic limit, calculated by $\sigma_{HEL} = \frac{1}{2}\rho_0 C_L u_{fs}|_A$, is about 6.8 GPa. The yield stress $\sigma_y$ is related to $\sigma_{HEL}$ via $\sigma_y = \sigma_{HEL}(1-2\nu)/(1-\nu)$, and $\sigma_y$ = 2.8 GPa.

The arrival of the release fan reflected from the free surface of the flyer plate leads to velocity decrease (*CD* in Fig. 1). The interaction of this release fan with that initiated from the target plate free surface releases the mid-part of the sample from compression into tension. Once the tensile stress exceeds a critical stress, termed as the spall strength $\sigma_{sp}$, spall occurs and is demonstrated on $u_{fs}$ as a re-acceleration (*DF*). The spall strength can be calculated as $\sigma_{sp} \approx \frac{1}{2}\rho_0 C_L \Delta u_{fs}$, here $\Delta u_{fs}$ is the difference in $u_{fs}$ between *C* and *D* (Fig. 1). The tensile strain rate can be estimated with $\dot{\varepsilon} \approx [du_{fs}(t)/dt]|_{release}/(2C_0)$. The spall strengths are estimated to be 4.4, 4.1, 4.5, and 4.7 GPa, in the order of increasing impact velocity. The tensile strain rates are about 4–5 × $10^5$ $s^{-1}$. $\sigma_{sp}$ for the incipient spall (LP389) shot is higher than the lowest full spallation shot (LP437), since the shock is purely elastic for the former and compression-induced damage is negligible. The re-acceleration is clearly composed of two stages, *DE* and *EF*, which represents growth and coalescence of isolated cracks or voids, respectively, and this feature is a characteristic of ductile fracture in general.

In order to investigate the microstructure of a shock-recovered sample, it is sectioned into two halves along the impact direction with a low-speed diamond saw, mechanically polished with 2000 grit silicon sand paper and 0.3 μm alumina particles. Fig. 2 shows SEM images of the cross-section of the shock-recovered sample (incipient spall, LP389). There is only a small crack, ~400 μm long, in the midsection [Fig. 2(a)]. Such incipient spall feature is consistent with the minor re-acceleration observed in the $u_{fs}(t)$ profile (*G* in Fig. 1). The crack shows a serrated profile rather than a straight line expected for brittle fracture, and certain regions of the crack remain partially connected [Fig. 2(b)]. We observe necking of the ligaments between neighboring voids [black arrows, Fig. 2 (c) and (d)]. The length of the ligaments is about 4–5 μm, and the narrowest width ($w_n$) is ~1 μm. We define the necking parameter as $\psi = (w_0 - w_n)/w_0 \times 100\%$, where $w_0$ is the original width. $\psi$ is about 65%. During tension, microvoids randomly nucleate and grow, and the ligaments between neighboring microvoids undergo ductile deformation via necking. These features are typical of plastic deformation, and demonstrate that some amount of plasticity can occur at micron level in this BMG under high strain-rate loading.

In addition to plastic deformation, softening is also observed as nanocones oriented nearly perpendicular to the local crack surface [Fig. 2(e)], and ductile dimples distributed uniformly on the fracture surface [white arrow, Fig. 2(f)]. Upon dynamic tension, viscosity near the spall plane is reduced to a level comparable to that of a liquid, allowing for the formation of a cone. Different local viscosities lead to various morphologies; higher viscosity corresponds to ductile dimples associated with considerable plasticity, while the cone feature reflects a lower viscosity. Necking and softening clearly demonstrate remarkable microscale plasticity and viscous flow during gas gun loading.

Higher impact velocities (369, 449, and 534 m $s^{-1}$) induce full spall, and the samples break in half along the spall plane. Fig. 3 presents SEM micrographs of spall fracture surfaces. Two distinct structures are common on the fracture surfaces, i.e., cup and cones, as shown in Fig. 3(a) and (b), respectively. Their sizes range from 10 to 200 μm. The depth profiles (red curves) for cups or cones are plotted in Fig. 3(a), (b), (f) and (g). Fig. 3(c) and (d) shows two important cup structures, and both contain a core-like center and vein-like patterns. Ridgelines (marked with white arrows) appear as the boundaries of the cups under tension. Around the core-like centers, shear bands (marked with black arrows) extend and terminate at a microvoid [marked with a circle, Fig. 3(h)] or a melted region near a microvoid [Fig. 3(i)]. Molten droplets of various sizes are found around the microvoid. Moreover, microvoids and molten droplets [Fig. 3(j)] similar to those in Fig. 3(i) are